Preresonance Raman Spectrum of the $C_{13}H_9$ Fluorene-like Radical

Jan Szczepanski, John Banisaukas, and Martin Vala*

Department of Chemistry and Center for Chemical Physics, University of Florida, Gainesville, Florida 32611-7200

So Hirata and William R. Wiley

Environmental Molecular Sciences Laboratory, Pacific Northwest National Laboratory, P.O. Box 999, Richland, Washington 99352

Received: March 27, 2002; In Final Form: May 23, 2002

The neutral open-shell species $C_{13}H_9$ formed from fluorene, $C_{13}H_{10}$, by low-energy electron bombardment and by ultraviolet photolysis in an argon matrix at 12 K has been studied via preresonance Raman, infrared, and ultraviolet/visible spectroscopy. Density functional theory calculations (B3LYP/6-31G(d,p)) of the CH bond energies of neutral fluorene showed that the most probable position for the hydrogen loss is the sp^3 carbon in the five-membered ring. Calculations of the $C_{13}H_9$ harmonic vibrational frequencies are shown to match the experimental Raman (and infrared) bands well. A new electronic transition is identified at 283.1 nm (4.38 eV). Its position agrees with earlier time-dependent density functional theory calculations. Oscillator strengths for this transition and three others are estimated. The electronic transitions in the dehydrogenated species, $C_{13}H_9$, are strongly red-shifted compared to fluorene.

I. Introduction

The species responsible for the unidentified infrared (UIR) emission bands observed from many carbon-rich interstellar sources and the carriers of the diffuse interstellar visible absorption bands (DIBs) have occupied researchers for many years now.[1−6] Polycyclic aromatic hydrocarbons (PAHs), in their neutral, ionized, hydrogenated, or dehydrogenated forms, have been proposed as possible carriers of both sets of bands. Since the PAHs were first proposed[1,2] as the primary UIR emitters in 1984−5, the model has been much discussed and many laboratory experiments and astrophysical observations and calculations have been performed, which point to the viability of the idea. Until recently, there were no direct measurements that showed that PAH ions could emit in the infrared or that PAHs were present in the interstellar medium. But now Cernicharo et al. have reported[7] infrared absorption bands in the vicinity of the protoplanetary nebula CRL 618, which they ascribe to the aromatic molecule, benzene. And, Saykally and co-workers have recently seen[8] the infrared emission from a PAH cation, pyrene, in a laboratory experiment.

Dehydrogenated and fragmented PAHs have been receiving an increasing amount of attention. Using Fourier transform ion cyclotron resonance (FT-ICR) mass spectrometry, Ekern and co-workers reported the loss of up to five hydrogens from the fluorene cation ($C_{13}H_{10}^+$) [9] and the complete dehydrogenation of the coronene cation ($C_{24}H_{12}^+$) and the naphthopyrene cation ($C_{24}H_{12}^+$)[10] after 1.5 s of UV (Xe lamp) photolysis. Recently, Dibben et al. demonstrated a similar photoprocess of stripping of H, C_2H_2, and C_4H_2 from fluorene cation to form pure C_9^+ and C_{11}^+ carbon clusters[11] in a proposed ring-opening mechanism.[12]

In this paper, we suggest that dehydrogenated PAHs may play a role in interstellar chemistry and could be responsible for some of the DIBs. It is general knowledge that, when ionized, neutral PAHs shift their electronic absorption bands to the red. But it is not widely known that removal of a hydrogen from a PAH may also result in a red shift. In general, lower-energy photons are required for hydrogen removal than for ionization of neutral PAHs. Thus, dehydrogenation could easily compete with ionization processes in regions of the interstellar medium (ISM) where penetration of low-temperature radiation is important. From recent laboratory experiments, it is now known that the photodehydrogenation of some PAH cations can occur very efficiently. Dehydrogenated neutral and ionic PAHs may therefore play a crucial role in the photochemistry of the ISM.

In this work, the spectral characterization of a neutral dehydrogenated PAH, $C_{13}H_9$, is presented. The $C_{13}H_9$ species was produced from fluorene ($C_{13}H_{10}$) by removal of one hydrogen (most likely from the sp^3 carbon) by either UV photolysis or low-energy electron bombardment. The Raman active modes were resonantly excited by 496.5 nm laser radiation, which corresponds to the low-energy absorption band shoulder of the $^2A_2(D_2) \leftarrow {}^2B_2(D_0)$ (0-0) transition of $C_{13}H_9$. This electronic transition was recently identified from a combination of experimental observations and vertical excitation energy calculations using time-dependent density functional theory (TDDFT).[13] The results of density functional theory (B3LYP/6-31G(d,p)) calculations of the harmonic frequencies of Raman and IR modes are also reported and compared to experimental data.

II. Computational Methods

Geometry optimization and calculation of harmonic frequencies for the $C_{13}H_9$ radical were carried out using density functional theory (DFT) employing the Becke3−Lee−Yang−Parr (B3LYP) functional with the 6-31G(d,p) basis set using

* To whom correspondence should be addressed. E-mail: mvala@chem.ufl.edu.

10.1021/jp020827a CCC: $22.00 © 2002 American Chemical Society
Published on Web 07/09/2002

the Gaussian 98 platform.[14] This level of theory has been demonstrated to be reliable in predicting mode frequencies and relative intensities of infrared absorption in medium-sized PAHs, even using lower-level basis sets.[15−16]

To determine the positions from which hydrogens are lost in $C_{13}H_{10}$, the C−H bond energies were estimated by subtracting the total energy of $C_{13}H_{10}$ from the total energy of the H and $C_{13}H_9$ products. All total energies were zero-point energy (ZPE) corrected. Adopted earlier for neutral and cationic fluorene, a scaling factor of 0.978 was used to compute the harmonic frequencies and zero-point energies for the $C_{13}H_9$ species. Its use resulted in good agreement between the calculated (B3LYP/6-31G(d,p)) and observed (Ar matrix, 12 K) mode frequencies.[12,13]

III. Experimental Methods

Fluorene ($C_{13}H_{10}$, Sigma) was sublimed into a vacuum chamber and, after mixing with Ar matrix gas, was deposited partially on the 12 K surface of an aluminum-coated copper block (for Raman studies) and partially on a 5 mm diameter BaF_2 window inserted in this block (for IR and UV/visible studies).

Two dehydrogenation procedures were used in this work: low-energy electron impact (EI) or UV photolysis (UVP). The electrons or UV photons crossed the fluorene/argon beam and, after transferring their energy to fluorene, resulted in H loss from $C_{13}H_{10}$. In the UVP method, the $C_{13}H_{10}$/Ar matrix was photolyzed using a 100 W medium-pressure Hg lamp with full spectral output ($h\nu$ < 5.5 eV). In the EI method, electrons emitted from the hot cathode of an electron gun were accelerated by a 300 V cathode-to-anode potential and collected by a +90 V O-ring electrode located on the front of the deposition block. Because the concentration ratio, [Ar]/[$C_{13}H_{10}$], is estimated to be ca. 1000, a great abundance of Ar* metastables is expected. Therefore, a high dehydrogenation yield is likely in the process:

$$Ar^* + C_{13}H_{10} \rightarrow Ar + C_{13}H_9(hot) + H$$

The $C_{13}H_9$ may release its excess energy either by electronic emission or by IR cascade emission or both. The dehydrogenation process will compete with the Penning ionization processes:

$$Ar^* + C_{13}H_{10} \rightarrow C_{13}H_{10}^{+} + e^{-} + Ar$$

and

$$Ar^* + C_{13}H_9 \rightarrow C_{13}H_9^{+} + e^{-} + Ar$$

In fact, all three products ($C_{13}H_9$, $C_{13}H_{10}^{+}$, and $C_{13}H_9^{+}$) were observed in the EI experiments. Their concentrations (compared to $C_{13}H_{10}$) were higher for larger Ar abundance in the $C_{13}H_{10}$/Ar beam.

Resonance Raman spectra were collected using a double Spex monochromator equipped with photon-counting detection. The 496.5 nm Ar^+ laser excitation light (50 mW) was spectrally prefiltered to remove the Ar^+ laser plasma lines and focused onto the matrix deposited on the Al-coated Cu block. The electronic absorption spectrum was recorded in a single-beam mode (through the sample/matrix trapped on the BaF_2 window) using the Raman system with a tungsten lamp. The infrared absorption spectrum was recorded in the 700−4000 cm^{-1} range

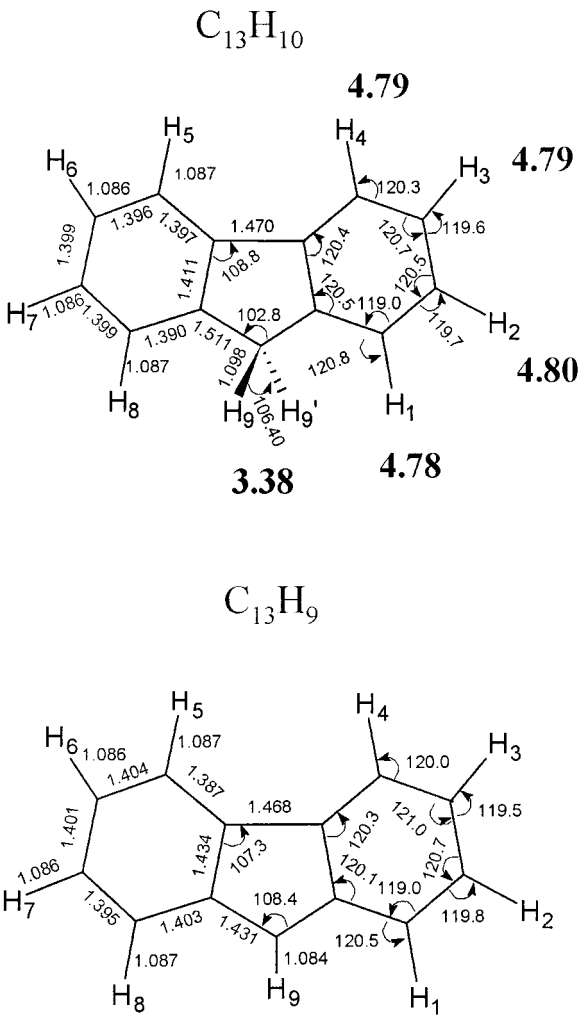

Figure 1. Optimized structures at the B3LYP/6-31G(d,p) level for the electronic ground state of $C_{13}H_{10}$ fluorene and $C_{13}H_9$ radical (formed from fluorene by $H_{9'}$ hydrogen loss from sp^3 carbon). The bond lengths (in Å) and the C−H bond energies (in eV, in bold type) estimated at B3LYP/6-31G(d,p) level are marked.

on the same sample/matrix using a MIDAC Fourier transform infrared (FTIR) spectrometer after simple 90° cryostat rotation.

IV. Results and Discussion

A. The C−H Bond Energies. The optimized structures for the parent fluorene ($C_{13}H_{10}$) and its dehydrogenated form ($C_{13}H_9$) are shown in Figure 1. Both structures possess C_{2v} symmetry. From the C−H bond energies of neutral fluorene, estimated at the B3LYP/6-31G(d,p) level and displayed in Figure 1, $H_{9'}$ (or its equivalent, H_9) is most likely the first hydrogen loss. The C−$H_{9'}$ bond energy is 3.38 vs 4.78 eV (or larger) for the other C−H_n (n = 1−8) bonds. The analogous bond energy in the fluorene $C_{13}H_{10}^{+}$ cation is 0.69 eV lower than 3.38 eV (as predicted by a previous B3LYP/6-31G(d,p) calculation[12]). This agrees with the observation of C−H bond energies of fluorene-like cationic fragments in ref 12 (cf. Figure 2) in which C−H bond energies were lower by ca. 0.3−0.7 eV for the open-shell compared to the closed-shell systems. These closed-shell vs open-shell differences in C−H bond energies result from the greater stability of the former systems.[17,18] The smaller C−$H_{9'}$ bond energy vs other C−H bond energies in $C_{13}H_{10}$ is consistent (cf. Figure 1) with its relatively long bond length (1.098 Å). After ejection of $H_{9'}$ from $C_{13}H_{10}$, the C−H_9 bond in $C_{13}H_9$ becomes the strongest and shortest of all of the

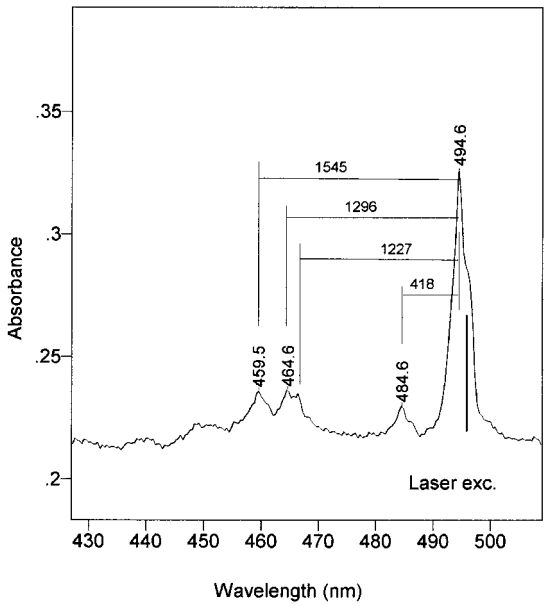

Figure 2. The $^2A_2(D_2) \leftarrow {}^2B_2(D_0)$ electronic absorption spectrum of the $C_{13}H_9$ radical isolated in Ar matrix at 12 K. The spectrum was recorded after 4 h matrix deposition during low-energy electron bombardment of the $C_{13}H_{10}$/Ar beam. The 496.5 nm Ar^+ laser line was used to resonantly excite the Raman vibrations (cf. Figure 3). Some vibrational mode frequencies (in cm^{-1}) active in the D_2 state are marked in the spectrum as well. Note that for the neutral $C_{13}H_9$ radical (an open-shell system) the lowest-energy spin- and symmetry-allowed electronic transition is red-shifted into the visible energy region from the ultraviolet region of the first electronic absorption of the parent fluorene.

C−H bonds in this species. A similar effect was observed earlier for the ionic system $C_{13}H_{10}^+/C_{13}H_9^+$, in which the C−$H_9$ bond in $C_{13}H_9^+$ was not broken in a number of different photofragmentation processes.[12,13] The potential energy curve along the C−$H_{9'}$ stretching coordinate was computed in the $C_{13}H_{10}$ ground electronic state to determine whether any energy barrier to the abstraction of the $H_{9'}$ atom was present. None was found. No barrier was found for the similar abstraction in the $C_{13}H_{10}^+$ cation either.

B. Preresonance Raman Spectrum. Because preresonance and resonance Raman spectra are affected only by the electronic ground-state vibrational modes, the $^2B_2(D_0)$ state harmonic mode frequencies were calculated (B3LYP/6-31G(d,p)) for the $C_{13}H_9$ species. These values, as well as the calculated Raman intensities, are compared to observed preresonance Raman bands in Table 1. The band intensity distribution is expected to be different in the preresonance Raman spectrum compared to the normal Raman distribution because of the intensity enhancement effect for the modes involved in the electronic transition. In fact, the 428 and 1575 cm^{-1} D_0 state modes (cf. Table 1 and Figure 3) are also observed in the electronic absorption to D_2 as 418 and 1545 cm^{-1} (cf. Figure 2), respectively. In the preresonance Raman spectrum, these modes increase their relative intensities from 0.02 and 0.01 (as predicted for normal Raman, cf. Table 1) to 1.0 and 0.9, respectively.

As usual with resonantly enhanced Raman modes, the overtone and combination modes observed in the spectrum of Figure 3 also have relatively large intensities. These involve the low-energy a_1 symmetry modes, 222, 428, and 883 cm^{-1} (cf. Table 1). The expected symmetry of the overtone and combination modes are a_1, because the direct product of $a_1 \times a_1 = a_1$ for C_{2v} symmetry. The intensity enhancement is observed for the 678, 1120, 1163, 1215, and 1368 cm^{-1} fundamental modes also.

TABLE 1: Preresonance Raman Band Assignments of Fluorene-like $C_{13}H_9$ Radical Observed in Solid Ar at 12 K (cf. Figure 3)[a]

	mode frequencies		intensities	
mode assignment[b]	obsd, cm^{-1}	calcd, cm^{-1}	obsd, rel	calcd, $Å^4$ amu^{-1}
τ(CCC) + ϵ(CH), a_1	222	212	0.13	4 (0.02)
τ(CCC) + β(CH), a_1	429 [418]	419	1.00	13 (0.05)
222 + 429	650		0.90	
ϵ(CH) + τ(CCC), b_1	678	696	0.20	2 (0.01)
ϵ(CH) + τ(CCC), a_2		742		4 (0.02)
2 × 429	849		0.16	
ϵ(CH) + τ(CCC)b_1		859		8 (0.04)
ϵ(CH) + τ(CCC)a_1	883	864	0.27	31 (0.12)
ϵ(CH) + τ(CCC)a_2		919		2 (0.02)
ϵ(CH) + τ(CCC)b_2		986		11 (0.04)
β(CH) + R(CC), a_1	1021	1020	0.07	65 (0.25)
222 + 2 × 429	1071		0.16	
β(CH) + R(CC), b_2		1092		13 (0.05)
222 + 883	1104		0.20	
β(CH) + R(CC), a_1	1120	1096	0.95	23 (0.09)
β(CH) + R(CC), a_1	1163	1156	0.40	25 (0.10)
β(CH) + R(CC), a_1	1194 [1227]	1192	0.90	227 (0.87)
β(CH) + R(CC), b_2	1215	1218	0.31	28 (0.10)
β(CH)+ R(CC), a_1	1256 [1296]	1249	0.87	262 (1.00)
β(CH)+ R(CC), a_1		1296		37 (0.14)
R(CC)+ βCH), b_2		1340		39 (0.15)
R(CC), a_1	1368	1370	0.41	41 (0.16)
R(CC), a_1	1443	1442	0.29	90 (0.34)
R(CC), b_2		1479		3 (0.01)
R(CC), a_1		1480		44 (0.17)
R(CC), b_2		1580		15 (0.06)
R(CC), a_1	1575 [1545]	1582	0.90	3 (0.01)
R(CC), b_2		1589		100 (0.38)

[a] The calculated Raman harmonic frequencies at B3LYP/6-31G(d,p) level for $^2B_2(D_0)$ ground state of $C_{13}H_9$ are scaled uniformly by 0.978 factor. All fundamental mode frequencies (in cm^{-1}) in the 100−1650 cm^{-1} range with Raman intensities equal to 2 $Å^4$/amu and larger are listed. The observed mode frequencies (in cm^{-1}) in the $^2A_2(D_2)$ electronic excited state are given in brackets, while the relative intensities are in parentheses. Note that the calculated normal Raman mode intensities are only loosely connected to the preresonance Raman band intensities (see text). [b] Notation used: R are stretching vibration modes, α and β are in-plane bending vibration modes, and ϵ and τ are out-of-plane vibration modes. The first vibration indicated, in modes of mixed character, contributes the largest amount to the total vibration. The mode symmetries in C_{2v} point group are given in the second column.

Geometry optimization (B3LYP/6-31G(d,p)) reveals that the fluorene skeleton is preserved in the $C_{13}H_9$ species. Because both $C_{13}H_9$ and $C_{13}H_{10}$ have the same symmetry (C_{2v}), similar mode frequencies and symmetries are expected. This expectation is realized. The Raman depolarization ratios, ρ, of the 221, 421, 846, 1022, 1093, 1156, 1195, 1238, 1349, 1480, and 1578 cm^{-1} bands determined by Bree and Zwarich for single-crystal fluorene lie in the range $0 < \rho < 0.75$, indicating that they all have a_1 symmetry.[19] These frequencies are in concert with the 222, 429, 883, 1021, 1120, 1163, 1194, 1256, 1368, 1443, and 1575 cm^{-1} frequencies observed here (cf. Figure 3). All are here assigned to a_1 symmetry (cf. Table 1). Two bands were observed in the Raman spectrum (cf. Figure 3) with mode symmetries different than a_1; one is of b_1 symmetry at 678 cm^{-1}, in close coincidence to the band calculated at 696 cm^{-1}, also of b_1 symmetry. The second one is of b_2 symmetry at 1215 cm^{-1} for which the predicted (B3LYP/6-31G(d,p)) band lies at 1218 cm^{-1} (b_2 symmetry, cf. Table 1). In the single-crystal

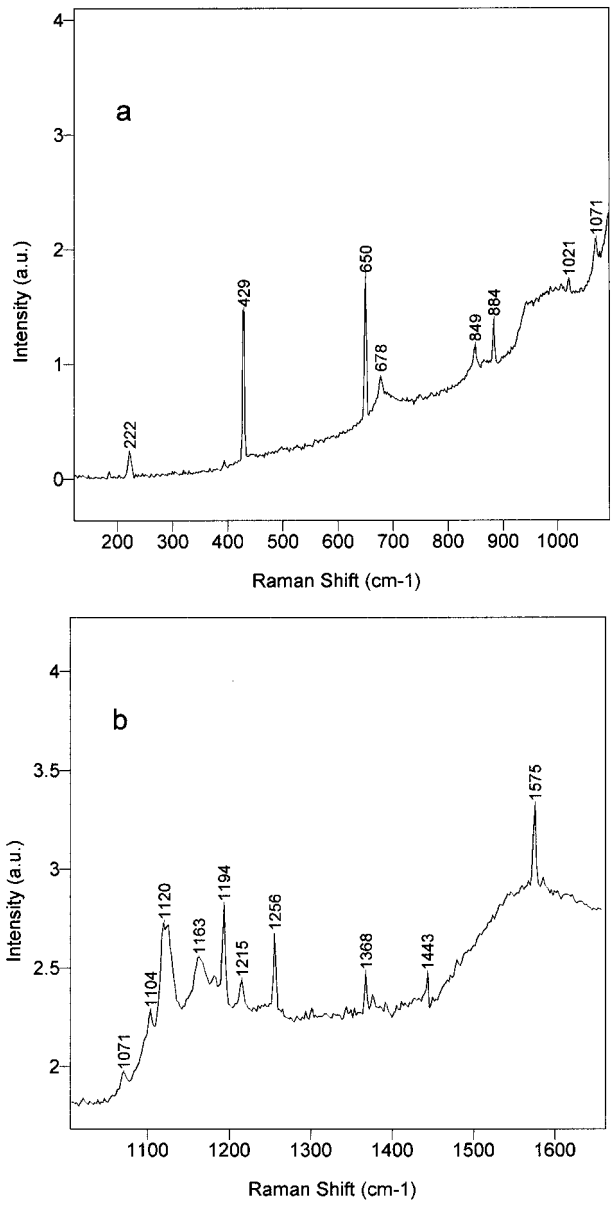

Figure 3. The preresonance Raman spectrum of $C_{13}H_9$ fluorene-like radical trapped in solid Ar at 12 K in the (a) 100−1100 and (b) 1000−1650 cm^{-1} regions. Laser excitation at 496.5 nm (50 mW) was used (cf. Figure 2). The Raman band shifts (in cm^{-1}) are marked. No resonantly enhanced Raman modes over 1600 cm^{-1} were observed (see text for the details).

Raman spectrum, two bands, 1193 and 1172 cm^{-1}, both of b_2 symmetry, were identified in this region.[19]

The preresonance Raman spectrum of the $C_{13}H_9$ species was scanned to 3200 cm^{-1}, but no bands in the region greater than 1600 cm^{-1} were observed. This is typical of the resonance Raman of aromatic species in which mostly resonantly enhanced ring modes but no C−H stretches are observed, even though in normal Raman spectra, these C−H modes are very strong. The resonance (or preresonance) Raman spectra of *p*-dichlorobenzene radical cation[20] and naphthalene radical cation [21] are good examples of this.

C. Infrared Absorption Spectrum. The IR and UV−visible absorption spectra were collected on the same $C_{13}H_9/C_{13}H_{10}$/Ar matrix. The infrared spectrum of the $C_{13}H_9$ radical revealed, in addition to the 722.2 and 780.9 cm^{-1} bands reported earlier,[13] new bands at 1239.5 and 1567.8 cm^{-1}. The intensities of the 1239.5 and 1567.8 cm^{-1} bands tracked the intensities of the former two bands under all experimental conditions used (i.e., EI with different electron beam energies and UVP with different photon fluxes). Intensities ratios of 1.0:0.98:0.10:0.43 for the 722.2, 780.9, 1239.5, and 1567.8 cm^{-1} bands were observed, respectively. From calculations, B3LYP/6-31G(d,p) (B3LYP/6-31++G(d,p)), harmonic IR frequencies (scaled by 0.978) were found at 725 [52 km/mol] (723 [94 km/mol]), 778 [44 km/mol] (785 [48 km/mol]), 1248 [10 km/mol] (1245 [10 km/mol]), and 1580 cm^{-1}[27 km/mol] (1572 cm^{-1}[31 km/mol]), with intensity ratios of 1.0(1.0):0.87(0.51):0.19(0.11):0.51(0.33), respectively. The agreement with experiment is very good.

D. Electronic Absorption Spectrum. A portion of the electronic absorption spectrum of the fluorene-like $C_{13}H_9$ radical was reported recently.[13] TDDFT (B3LYP/6-31(2+,2+)G(d,p)) calculations[13] predicted a $^2A_2 \leftarrow {}^2B_2(D_0)$ electronic transition in $C_{13}H_9$ at 4.37 eV ($f_{TDDFT} = 0.0154$) that was not observed in our earlier work. An extended search for such a band in a series of experiments in the UV−vis−IR regions (on the same $C_{13}H_9$/Ar matrices) revealed a candidate at 283.1 nm (4.38 eV). This band (cf. Figure 4b) displayed parallel intensity behavior with the previously assigned 494.6 (2.51), 370.6 (3.34), and 353.2 nm (3.51 eV) bands, as well as the 722.2, 780.9, 1239.5, and 1580 cm^{-1} infrared bands, all attributed to $C_{13}H_9$ radical. It is concluded that the 283.1 nm band is the predicted $^2A_2 \leftarrow {}^2B_2(D_0)$ 0-0 transition in $C_{13}H_9$.

Because the electronic and IR absorption spectra were recorded on the same sample/matrices in the above experiments, it is possible to determine the oscillator strengths of the optical bands. The experimental ratio of the $^2A_2(D_2) \leftarrow {}^2B_2(D_0)$ (0-0) absorption transition (494.6 nm) and the 780.9 cm^{-1} absorption (well-isolated IR band, not displayed) was determined as $A(494.6)/A(780.9) = 43.6$. Assuming that the B3LYP/6-31G(d,p) integral intensity of 44 km/mol $= 2.303\epsilon_{max}(780.9)\Delta\nu_{1/2}$ for the 778 cm^{-1} (780.9 cm^{-1} experimental) band is reliable, the molar absorption coefficient, $\epsilon_{max}(494.6)$, of the 494.6 nm $C_{13}H_9$ band is found equal to 33 340 M^{-1} cm^{-1}. From this value, an oscillator strength, $f_{est} = 0.025$, was estimated for the experimental absorption spectrum in Figure 2. With the use of the B3LYP functional with the diffuse functions added to the basis set (B3LYP/6-31++G(d,p)), a 10% increase in the integral intensity of the calculated 785 cm^{-1} band was observed. This increase reflects a similar increase for all f_{est} values in Table 2, when B3LYP/6-31++G(d,p) is applied in the oscillator strength estimated. The spectrum was assigned[13] to the $^2A_2(D_2) \leftarrow {}^2B_2(D_0)$ transition of $C_{13}H_9$ from TDDFT calculations, which predicted an oscillator strength of $f_{TDDFT} = 0.0525$. Using similar procedures, we also estimated the oscillator strengths of the other absorption bands in the Figure 4. The values are given in Table 2.

V. Conclusions

(1) On the basis of the calculated low energy (3.38 eV) for the $C-H_{9'}$ bond in $C_{13}H_{10}$, the first dehydrogenation in fluorene is most likely the loss of $H_{9'}$ from the sp^3 carbon.

(2) The preresonance Raman spectrum of the fluorene-like $C_{13}H_9$ radical was recorded and analyzed. Density functional theory calculations (B3LYP/6-31G(d,p)) of the harmonic mode frequencies are shown to agree well (after scaling) with the observed band positions. Vibrational mode symmetries agree with the assignments of fundamentals reported for single-crystal fluorene.

(3) Two new infrared bands at 1239.5 and 1567.8 cm^{-1}, together with the previously observed 722.2 and 780.9 cm^{-1} bands, were identified as arising from the $C_{13}H_9$ radical in solid Ar.

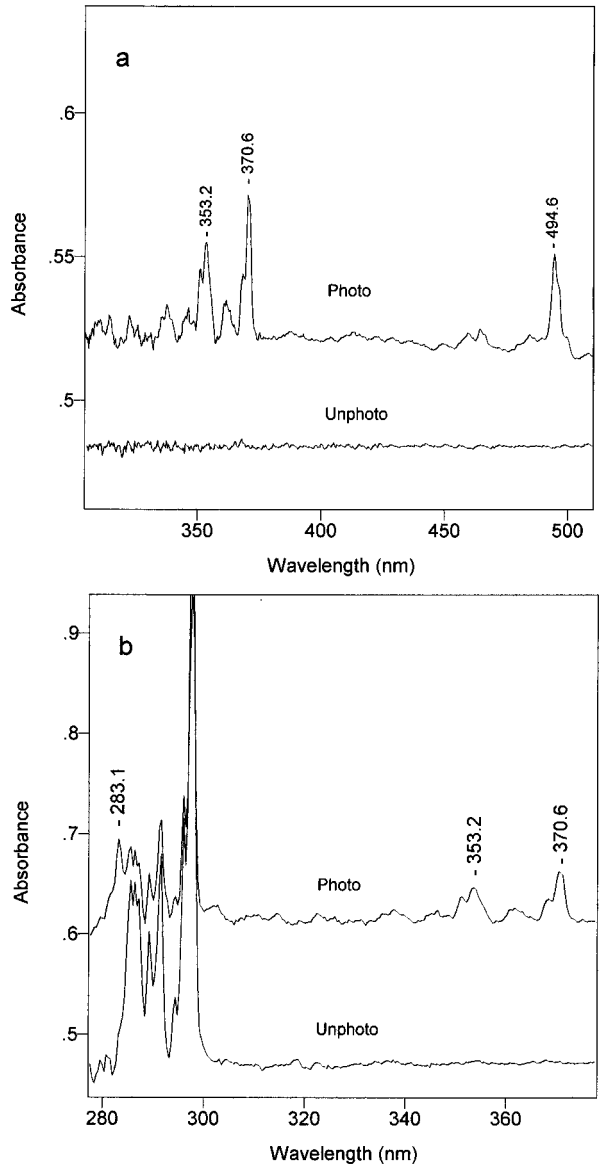

Figure 4. Part of the electronic absorption spectrum of fluorene neutral, $C_{13}H_{10}$, isolated in solid Ar at 12 K (before UV photolysis, lower spectrum) and the absorption spectrum of the mixture of $C_{13}H_{10}$ and $C_{13}H_9$ fluorene-like radical in solid Ar (recorded after 2 h of photolysis of $C_{13}H_{10}$/Ar matrix) displayed in two energy regions: (a) 340−500 nm; (b) 280−370 nm. The marked bands, attributed to the $C_{13}H_9$ radical, are assigned in Table 2. The strong band at 297.5 nm is due to the $S_1 \leftarrow S_0$ (0-0) transition of parent fluorene. These spectra are baseline-corrected to cancel the steadily rising signal with decreasing wavelength due to Rayleigh scattering. Note the ca. 50% intensity decline of the parent fluorene bands after UV photolysis.

(4) The newly observed UV band at 283.1 nm was tentatively assigned to a $^2A_2 \leftarrow {}^2B_2(D_0)$ transition of the $C_{13}H_9$ radical on the basis of the energy coincidence with the calculated vertical excitation energies[13] as well as of band intensity correlations with the known bands of $C_{13}H_9$. From the intensity-correlated IR and UV−visible bands (recorded on the same $C_{13}H_9$/Ar matrix) and from the calculated (B3LYP/6-31G(d,p)) IR integral band intensities, the oscillator strengths, f_{est}, for the observed UV−visible bands were estimated and shown to compare reasonably well with the calculated f_{TDDFT} values.

(5) The preresonance Raman spectrum obtained with 496.5 nm laser excitation combined with calculated Raman frequencies of $C_{13}H_9$ confirms the earlier assignment of the $^2A_2(D_2) \leftarrow {}^2B_2(D_0)$ (0-0) absorption transition at 494.6 nm (in solid Ar) to the $C_{13}H_9$ fluorene-like radical.

TABLE 2: Oscillator Strength Values, f_{est}, Estimated from the Intensity-Correlated IR and UV−Visible Bands (recorded on the same $C_{13}H_9$/Ar Matrix) and from the Calculated (B3LYP/6-31G(d, p)) IR Band Integral Intensities[a]

	calcd[b]		expt	
state[b]	energy, eV	f_{TDDFT}	energy, eV (nm)	f_{est}[c]
$^2A_2$ ($\pi_0 \leftarrow \pi_{-2}$)	2.75	0.0525	2.51 (494.6)[b]	0.025
$^2B_2$ ($\pi_0 \leftarrow \pi_{-4}$)	3.69	0.0153	3.34 (370.6)[b]	>0.050[d]
$^2A_2$ ($\pi_2 \leftarrow \pi_0$)	3.93	0.0359	3.51 (353.2)[b]	< 0.037[d]
$^2A_2$ ($\pi_1 \leftarrow \pi_{-2}$)	4.37	0.0154	4.38 (283.1)[c]	>0.012[e]

[a] The calculated f_{TDDFT} oscillator strengths for fluorene-like $C_{13}H_9$ radical using TDDFT with B3LYP functional and 6-31(2+,2+)G(d,p) basis set are given for the sake of comparison. TDDFT vertical excitation energies (eV) and experimental 0-0 absorption band positions (eV (nm)) from the $^2B_2$ ground state are listed. [b] From ref 13. [c] This work. The f_{est} values are 10% higher when the B3LYP/6-311++G(d,p) level is applied. [d] The uncertain f_{est} value is due to partial overlap with the $^2B_2 \leftarrow {}^2B_2(D_0)$ or $^2A_2 \leftarrow {}^2B_2(D_0)$ transition (cf. Figure 4a). [e] f_{est} value error is due to the lack of observation of high-energy vibrational progression bands for this transition and blending with the parent fluorene $S_1 \leftarrow S_0$ absorption bands (cf. Figure 4b).

It is well-known that upon ionization the electronic absorption spectra of many PAHs undergo a considerable red-shift. We have shown here that a similar red-shift occurs in the neutral open-shell system $C_{13}H_9$ upon single hydrogen loss from the parent fluorene. The lowest-energy spin- and symmetry-allowed electronic transition is shifted from the ultraviolet into the visible region after the loss of one hydrogen. This is apparently typical for small and medium-sized closed-shell PAH neutrals. Radziszewski observed that dehydrogenated neutral benzene radical shifted its lowest electronic absorption into the visible region.[22] Because PAH cations possess strong electronic absorption bands in the visible region, they were originally proposed as possible carriers of some of the diffuse interstellar bands (DIBs).[23−25] The DIBs are a series of over 200 absorption bands of varying bandwidth observed from many regions of interstellar space where high carbon abundances are expected. If the observation reported here, that dehydrogenation of neutral closed-shell PAHs yielding neutral open-shell systems exhibiting bands red-shifted into the visible, can be shown to be a general phenomenon, these systems may then need to also be considered carefully as possible carriers of the DIBs.

Acknowledgment. The authors acknowledge the Petroleum Research Foundation, administered by the American Chemical Society, for its support of this research and the Northeast Regional Data Center for a grant under the Research Computing Initiative for computer time.

References and Notes

(1) Leger, A.; Puget, J. L. *Astron. Astrophys.* **1984**, *137*, L5.

(2) Allamandola, L. J.; Tielens, A. G. G. M.; Barker, J. R. *Astrophys. J.* **1985**, *290*, L25.

(3) Russel, R.; Soifer, B.; Willner, W. *Astrophys. J.* **1977**, *217*, L149; **1978**, *220*, 568.

(4) Szczepanski, J.; Vala, M. *Nature* **1993**, *363*, 699.

(5) Joblin, C.; Tielens, A. G. G. M.; Geballe, T. R.; Wooden, D. H. *Astrophys. J.* **1996**, *460*, L119−L122.

(6) Snow, T. P.; Page, V. L.; Keheyan, Y.; Bierbaum, V. *Nature* **1998**, *391*, 259.

(7) Cernicharo, J.; Heras, A. M.; Tielens, A. G. G. M.; Pardo, J. R.; Herpin, F.; Guelin, M.; Waters, L. B. F. M. *Astrophys. J.* **2001**, *546*, L123−L126.

(8) Kim, H. S.; Wagner, D. R.; Saykally, R. J. *Phys. Rev. Lett.* **2001**, *86*, 5691.
(9) Ekern, S. P.; Marshall, A. G.; Szczepanski, J.; Vala, M. *J. Phys. Chem. A* **1998**, *102*, 3498.
(10) Ekern, S. P.; Marshall, A. G.; Szczepanski, J.; Vala, M. *Astrophys. J.* **1997**, *L39*−*L41*, 488.
(11) Dibben, M. J.; Kage, D.; Szczepanski, J.; Eyler, J. R.; Vala, M. *J. Phys. Chem. A* **2001**, *105*, 6024.
(12) Szczepanski, J.; Dibben, M. J.; Pearson, W.; Eyler, J. R.; Vala, M. *J. Phys. Chem. A* **2001**, *105*, 9388.
(13) Szczepanski, J.; Banisaukas, J.; Vala, M.; Hirata, S.; Bartlett, R. J.; Head-Gordon, M. *J. Phys. Chem. A* **2002**, *106*, 63.
(14) Frisch, M. J.; Trucks, G. W.; Schlegel, H. B.; Scuseria, G. E.; Robb, M. A.; Cheeseman, J. R.; Zakrzewski, V. G.; Montgomery, J. A., Jr.; Stratmann, R. E.; Burant, J. C.; Dapprich, S.; Millam, J. M.; Daniels, A. D.; Kudin, K. N.; Strain, M. C.; Farkas, O.; Tomasi, J.; Barone, V.; Cossi, M.; Cammi, R.; Mennucci, B.; Pomelli, C.; Adamo, C.; Clifford, S.; Ochterski, J.; Petersson, G. A.; Ayala, P. Y.; Cui, Q.; Morokuma, K.; Malick, D. K.; Rabuck, A. D.; Raghavachari, K.; Foresman, J. B.; Cioslowski, J.; Ortiz, J. V.; Stefanov, B. B.; Liu, G.; Liashenko, A.; Piskorz, P.; Komaromi, I.; Gomperts, R.; Martin, R. L.; Fox, D. J.; Keith, T.; Al-Laham, M. A.; Peng, C. Y.; Nanayakkara, A.; Gonzalez, C.; Challacombe, M.; Gill, P. M. W.; Johnson, B. G.; Chen, W.; Wong, M. W.; Andres, J. L.; Head-Gordon, M.; Replogle, E. S.; Pople, J. A. *Gaussian 98*, revision A.3; Gaussian, Inc.: Pittsburgh, PA, 1998.
(15) Bauschlicher, C. W., Jr. *Astrophys. J.* **1998**, *509*, L125−L127 and references therein.
(16) Langhoff, S. R. *J. Phys. Chem.* **1996**, *100*, 2819.
(17) Hudgins, D. M.; Bauschlicher, C. W.; Allamandola, L. J. *Spectrochim. Acta A* **2001**, *57*, 907.
(18) Weisman, J. L.; Lee, T. J.; Head-Gordon, M. *Spectrochim. Acta A* **2001**, *57*, 931.
(19) Bree, A.; Zwarich, R. *J. Chem. Phys.* **1969**, *51*, 903.
(20) Szczepanski, J.; Personette, W.; Pellow, R.; Chandrashekar, T. M.; Roser, D.; Cory, M.; Zerner, M.; Vala, M. *J. Chem. Phys.* **1992**, *96*, 35.
(21) Kawashima, H.; Kato, T.; Shida, T. *Chem. Phys. Lett.* **1990**, *165*, 59.
(22) Radziszewski, J. G. *Chem. Phys. Lett.* **1999**, *301*, 565.
(23) van der Zwet, G. P.; Allamandola, L. J. *Astron. Astrophys.* **1985**, *146*, 76.
(24) Leger, A.; d′Hendecourt, L. *Astron. Astrophys.* **1985**, *146*, 81.
(25) Crawford, M. K.; Tielens, A. G. G. M.; Allamandola, L. J. *Astrophys. J.* **1985**, *293*, L45.